Absolute CO number densities measured using TALIF in a non-thermal plasma environment

Please check the document version of this publication:

Absolute CO number densities measured using TALIF in a non-thermal plasma environment

IOP ebooks™

Bringing you innovative digital publishing with leading voices to create your essential collection of books in STEM research.

Start exploring the collection - download the first chapter of every title for free.

Absolute CO number densities measured using TALIF in a non-thermal plasma environment

M A Damen[ID]**, D A C M Hage, A W van de Steeg**[1]**[ID]**, **L M Martini**[ID] **and R Engeln**[ID]

Department of Applied Physics, Eindhoven University of Technology, 5600MB Eindhoven, The Netherlands

E-mail: r.engeln@tue.nl

Abstract

We report first measurements of time-resolved absolute CO number densities and rotational temperatures in a non-thermal CO_2 plasma environment using TALIF with a nanosecond pulsed laser. Two-photon excitation spectra from the $B^1\Sigma^+(v'=0) \leftarrow X^1\Sigma^+(v''=0)$ Q-branch are recorded and fitted to extract rotational temperatures. Absolute number densities are determined from the frequency-integrated excitation spectrum. The plasma under investigation is a pulsed glow discharge operated at a frequency of 60 Hz with an plasma-on time of 5 ms per plasma cycle, 50 mA plasma current and a pressure of 6.67 mbar. CO number densities range from $(2.6 \pm 0.6) \times 10^{22}$ m^{-3} to $(1.2 \pm 0.3) \times 10^{22}$ m^{-3}, while rotational temperatures range from 370 ± 40 K to 700 ± 70 K at the beginning and end of the plasma-on phase, respectively. Our results show fair agreement with literature data.

Keywords: carbon dioxide plasma, glow discharge, two-photon absorption laser-induced fluorescence, carbon monoxide, absolute number densities, rotational temperatures

1. Introduction

Two-photon absorption laser-induced fluorescence (TALIF) is a spectroscopic technique that allows species-selective ground-state number densities to be determined with a high space and time resolution for species that require high energy photons for electronic excitation. Absorption of two photons can be used to make these high-lying electronic energy levels accessible without the need for experimentally challenging VUV excitation wavelengths. TALIF is hence typically applied to atomic species like hydrogen [1, 2], nitrogen [2–4] or oxygen [2, 5, 6]. However, two-photon excitation is also required for some molecular species like CO, which has relatively high-lying electronic states [7, 8]. Some TALIF measurements have already been performed on CO in combustion studies because of its low CO detection limit [9, 10].

To the authors knowledge, no TALIF studies on CO in a (non-thermal) plasma environment have yet been reported.

While Raman scattering can measure both the rotational temperature and CO number density spatially and temporally resolved [11–13], CO sensitivity is low in a CO_2 environment using Raman scattering due to crosstalk from CO_2 [13]. Similarly, absorption techniques using tunable infrared lasers or fourier-transform infrared spectroscopy provide line-of-sight instead of spatially resolved measurements and typically do not allow nanosecond time resolutions. TALIF on CO provides both the high spatial and temporal resolution, while also being species selective (in both excitation and detection), making the technique well suited for rotational temperature and CO number density measurements in a CO_2-rich environment.

Many of the studies on TALIF applied to CO report on two-photon absorption using the $B^1\Sigma^+(v'=0) \leftarrow X^1\Sigma^+(v''=0)$ Q-branch [7, 14, 15], with fluorescence being detected from the $B^1\Sigma^+(v'=0) \rightarrow A^1\Pi(v'')$ transition (450–700 nm). Alternatively, some investigations use the $C^1\Sigma^+(v'=0) \leftarrow X^1\Sigma^+(v''=0)$

Q-branch for excitation, since this eliminates potential single-photon absorption crosstalk from C_2 at 230 nm without a significant impact on fluorescence yield [7, 10, 16]. Excitation to the $B^1\Sigma^+$ state however has the advantage of having well documented quenching rates and level constants of the $B^1\Sigma^+$ state, in contrast to the $C^1\Sigma^+$ electronic level. Hence, excitation to the $B^1\Sigma^+$ state is employed in this study.

The aim of this paper is to measure time-resolved absolute number densities of CO in a CO_2 glow discharge. These glow discharges are well studied, both historically for their application in CO_2 lasers [17–19] and more recently to study CO_2 vibrational kinetics [13, 20, 21] for the synthesis of solar fuels [22–24]. Due to its uniformity in the positive column, CO number densities have been measured with both absorption spectroscopy [20, 25] and rotational Raman spectroscopy [13]. This allows comparison of measured temporally resolved CO number densities using TALIF with previously reported number densities. Furthermore, a glow discharge can be operated in a favourable pressure window of a few millibars, avoiding radiative trapping at lower pressures [14] while minimizing non-radiative losses from the electronically exited state at higher pressures.

2. Experimental methods

2.1. Excitation and detection system

The experimental setup is shown schematically in figure 1(a). A frequency tripled nanosecond pulsed Nd:YAG laser (Spectra Physics Quanta Ray PRO 290-30) was used to pump a dye laser (Sirah PrecisionScan, Coumarin 460 dye) and create vertically polarized light with a tunable wavelength around 460 nm. The dye laser output was frequency doubled using a SHG BBO crystal to generate a tunable wavelength around 230 nm with a spectral width of about $0.18\ \mathrm{cm}^{-1}$ and an energy of 10 μJ per pulse.

The laser beam was focussed into the center of the plasma reactor (both longitudinally and radially) using a combination of a negative ($f = -200$ mm) and positive lens ($f = 100$ mm). Fluorescence at the laser focus was collected by a lens ($f = 35$ mm), spatially filtered by an iris and focused into a glass fiber with a diameter of $200\ \mu$m by a second lens ($f = 30$ mm). Light from the fiber passed through a bandpass filter (Thorlabs FB520-10, FWHM 10 nm) centered at 520 nm, thus only detecting the $B^1\Sigma^+(v'=0) \rightarrow A^1\Pi(v''=2)$ transition to minimize detection of plasma emission. Fluorescence from this band was detected using a photomultiplier tube (Hamamatsu R12829) and recorded by an oscilloscope (Keysight DSOX3034T).

2.2. Plasma setup

The plasma reactor that was used in this study is shown schematically in figure 1(a) and is made of Pyrex. It consists of a 18.5 cm long cylinder with a 2 cm internal diameter, extending at both ends 2.5 cm into a Pyrex KF40 adapter, resulting in a total internal reactor length of 23.7 cm. The
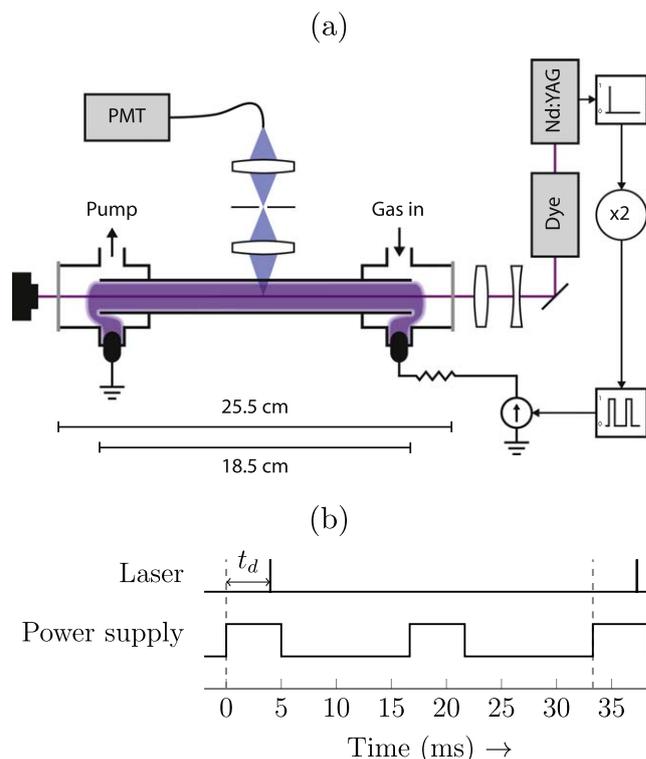

Figure 1. A schematic representation of the TALIF setup in (a), where the tunable excitation wavelength was generated by a combination of a Nd:YAG laser, a tunable dye laser and a frequency doubling crystal. The laser beam was focussed into a Pyrex reactor, where the fluorescence was collected at a 90° angle and focussed into a glass fiber. The fiber was connected to a photomultiplier tube and a oscilloscope to record the fluorescence signal. The pulse delay generator was used to generate two plasma cycles for each laser pulse, as shown in (b). The laser pulse was shifted by a time t_d with respect to the start of the plasma cycle.

high voltage and grounded electrodes are spaced 16 cm apart and are placed opposite to gas inlet and outlet, respectively.

The high voltage electrode was connected via a 50 kΩ resistor to a high-voltage power amplifier (Trek 10/40A-HS) operating in constant current mode at 50 mA. A pulse delay generator (Stanford Research Systems DG535) was used to provide the triggers (both lamps and Q-switch) at the operating frequency of the laser (30 Hz). The same pulse delay generator was used to generate two plasma cycles with a 5 ms on-time and a 11.67 ms off-time each (60 Hz) upon each laser shot, as illustrated in figure 1(b). The respective plasma on-time was chosen in accordance with experiments performed by Klarenaar *et al* [20], while the repetition rate of the plasma was chosen as twice the laser repetition rate.

A pure CO_2 gas flow (Linde 4.5 Instrument, $\geqslant$99.995% purity) of 7.4 sccm was supplied using a mass flow controller (Bronkhorst F-201CV). This leads to a plasma residence time of a few seconds, where the molecules experience about 100 plasma cycles on average before exiting the active region of the discharge. The pressure was kept constant at 6.67 mbar by automatically adjusting the effective pumping speed of a dry Roots pump (Pfeiffer ACP 15) through control of an automatic valve (Pfeiffer EVR 116) using a feedback controller (Pfeiffer RVC 300) and a pressure gauge (Pfeiffer CMR 263).

Conditions were very similar to work performed by Klarenaar *et al*, including pressure, gas flow and plasma current and thus similar reduced electric fields of about 60 Td are expected [20].

2.3. Experimental procedure

Custom software was used to perform a stepwise scan of the excitation frequency and to subsequently record the fluorescence averaged over 128 laser shots. The fluorescence was corrected for any background illumination, integrated over time and then combined into an excitation spectrum. An excitation spectrum in pure CO at room temperature was recorded for intensity, laser linewidth and wavelength calibration. The plasma cycle was subsequently started, allowing approximately 5 min for stabilization of the plasma before measuring an excitation spectrum at a given time delay t_d with respect to the start of the plasma cycle. Laser energy measurements were performed using a power meter for both the reference measurement and time-series in the plasma to allow correction for changes in laser energy over time.

3. Theory

3.1. Spectral profile of fluorescence

The spectral profile of the measured two-photon excitation spectrum depends on the rotational temperature, with rotational lines of CO typically being convoluted due to pressure and Doppler broadening. The limited linewidth of a nanosecond laser system however allows rotational temperatures to be extracted from the fluorescence emission rate I_f using a fitting procedure for the full excitation spectrum. At our experimental conditions, Doppler broadening is typically one order of magnitude larger than pressure broadening and similar to the laser broadening. Hence a further improvement on the resolvability of the rotational lines can be achieved by measuring Doppler-free excitation spectra, although this is experimentally challenging [5, 26].

For a given electronic transition $j \rightarrow k$, this emission rate I_r is proportional to the product of the Stern–Volmer factor describing fluorescence yield, the photon flux density $\tilde{I}$ in $m^{-2}\,s^{-1}$, two-photon rate coefficient $\hat{\sigma}^{(2)}$ in $m^4\,s^1$ and the CO number density N_0 in m^{-3} [15, 27]:

$$I_f \propto \frac{A_{jk}}{Q + R\tilde{I} + \sum_{i \neq j} A_{ji}} \hat{\sigma}^{(2)} (\tilde{I})^2 N_0. \tag{1}$$

Here A_{ji} is the Einstein A coefficient for spontaneous emission, Q is the total collisional quenching frequency and R is the single-photon ionization rate coefficient. It was experimentally verified that the fluorescence scales with the square of the laser power and hence it can be concluded that the product of $R\tilde{I}$ is negligible compared to the quenching frequency Q and the sum of the Einstein A coefficients at our pulse energies. A significant ionization contribution would result in a sub-quadratic scaling. Additionally, this confirms

that the ground state is not significantly depleted (analogues to the linear regime in single-photon absorption) [28].

It has been shown by Di Teodoro *et al* that the quenching frequency Q for the $B^1\Sigma^+$ state does not depend on the rotational level J [14], and therefore the spectral profile of I_f is fully determined by the two-photon rate coefficient $\hat{\sigma}^{(2)}$. Calculation of this two-photon rate coefficient follows the method reported by Di Rosa *et al* [15], where the O and S branches are omitted. The absence of these branches was verified experimentally and is supported by calculations of two-photon Hönl–London factors [29] (see appendix). The calculations show Q-branch transition strengths to be over two orders of magnitude larger than those of the O and S branches for all $J \neq 0$ for a typical ratio of linearly and circularly polarized light S_{ll}^Q / S_{cc}^Q of 200 [30].

3.2. Collisional quenching

While direct measurement of the quenching parameter from the effective lifetime is preferred, this is not possible since the nanosecond laser pulse duration is longer than expected effective lifetimes. Additionally, radiation trapping of $B^1\Sigma^+ \rightarrow X^1\Sigma^+$ radiation can cause the effective lifetime to exceed the natural lifetime [14], significantly complicating the extraction of the quenching frequency from the effective lifetime. The quenching frequency Q is hence calculated from known quenching rate coefficients and an estimate for the plasma conversion. This plasma conversion factor α is defined as

$$\alpha = \frac{[CO]}{[CO] + [CO_2]}, \tag{2}$$

where [CO] and [CO₂] are the molecular number densities of CO and CO₂, respectively. It has been shown previously that the global and local gas mixture are identical (i.e. good mixing between the species is present in the reactor) [13, 20]. From the CO₂ dissociation reaction $2CO_2 \rightarrow 2CO + O_2$ it is assumed that for every two molecules of CO₂, two molecules of CO and a single molecule of O₂ are formed. Although atomic oxygen is also likely formed [31], its number density is expected to be very low with respect to molecular oxygen and thus its contribution to the quenching frequency is neglected [32]. From this dissociation reaction, the molecular fraction of CO₂ (f_{CO_2}) can be calculated

$$f_{CO_2} = \frac{1 - \alpha}{1 + \alpha/2}. \tag{3}$$

Similarly, the molecular fractions for CO and O₂ are given by $f_{CO} = \frac{\alpha}{1 + \alpha/2}$ and $f_{O_2} = \frac{\alpha/2}{1 + \alpha/2}$, respectively. Given these molecular fraction equations, the total quenching frequency Q is

$$Q = (q_{CO_2} f_{CO_2} + q_{CO} f_{CO} + q_{O_2} f_{O_2})p \tag{4}$$

with q_{CO_2}, q_{CO} and q_{O_2} temperature-dependent quenching rate coefficients [33] and p the total pressure. Here, CO₂ manifests the highest collisional quenching rate with respect to O₂ and CO, with quenching rate coefficients of 19.9, 14.1 and 6.0 MHz mbar^{-1}, respectively, at 296 K.
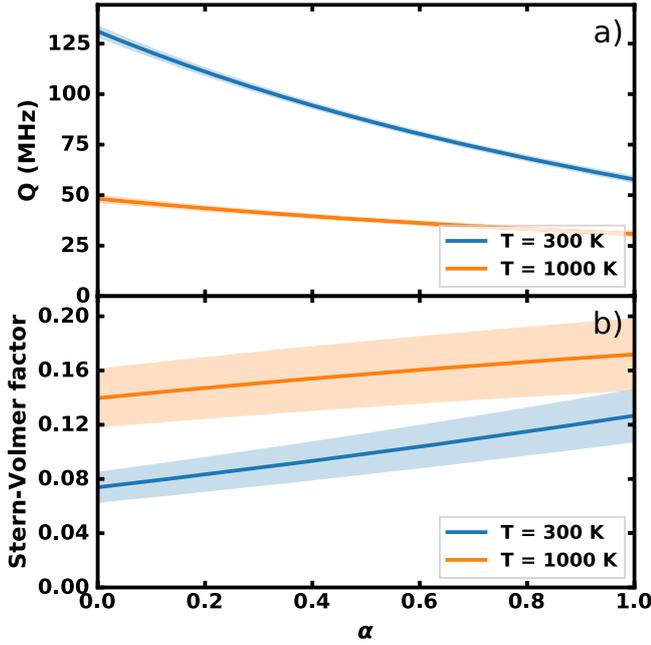
Figure 2. An example of calculated quenching frequencies in (a) and Stern–Volmer factors in (b), as a function of the plasma conversion parameter α at temperatures of 300 K and 1000 K. The Stern–Volmer factor increases with increasing plasma conversion as a result of the lower quenching rate coefficients of CO and O_2 with respect to CO_2. Shaded regions represent the (systematic) uncertainties in the calculated values as a result of literature data uncertainties.

Figure 2(a) shows calculated quenching frequencies as a function of the plasma conversion factor α for two different temperatures, while figure 2(b) shows the related Stern–Volmer factors. Klarenaar *et al* [20] found a conversion of $\alpha = 0.18$ in a very similar plasma. Even when taking our initial estimation for the plasma conversion $\tilde{\alpha}$ in the range of $0 < \tilde{\alpha} < 0.36$, the Stern–Volmer factor only varies by 12% over this range at 300 K and 9% at 1000 K. A rough indication of the plasma conversion $\tilde{\alpha}$ is thus sufficient to estimate the $B^1\Sigma^+$ quenching frequencies, which in turn allows CO number densities to be determined within reasonable accuracy. This is generally true for systems with limited changes in gas composition or similar quenching rate coefficients for the reactants and products. The plasma conversion α can subsequently be determined with a significantly smaller error margin than the initial plasma conversion estimation $\tilde{\alpha}$.

4. Computational methods

To be able to analyze measured excitation spectra, a computational procedure has been developed to calculate and fit these excitation spectra to extract the rotational temperature and spectral integral of the excitation spectrum. The fitting function decouples the excitation spectrum into a normalized shape $\Phi(\Omega_c)$ and its amplitude Γ and is thus given by $\mathcal{F}(\Omega_c) = \Gamma\Phi(\Omega_c) + \Gamma_0$. Here Γ_0 is introduced as an adjustable fitting parameter to account for the intensity offset resulting

from detected plasma emission and/or stray light. The normalized spectral shape Φ as a function of the two-photon excitation frequency Ω_c is given by

$$\Phi(\Omega_c) = \hat{\sigma}^{(2)}(\Omega_c) / \int_0^\infty \hat{\sigma}^{(2)}(\Omega_c)\mathrm{d}\Omega_c. \quad (5)$$

Frequencies of rotational lines are calculated from the electronic level spacing E and the rotational and centrifugal constants B and D of the lower and upper electronic state, respectively, [8] and an empirical relation for the pressure shift [34]. Line profiles are represented using a Voigt profile, including contributions for Doppler broadening and an empirical relation for pressure broadening [34]. Furthermore, we assume a constant spectral laser profile over the full Q-branch, as well as J-independent Doppler and pressure broadening. The rotational temperature T_{rot} is assumed to be equal to the gas temperature T [17] and the pressure is measured directly using a pressure gauge. The effective spectral laser width is determined by fitting a room-temperature excitation spectrum with a high signal-to-noise ratio and is subsequently fixed for plasma measurements.

The computational algorithm is tested on data from literature by Di Rosa *et al* [15] at room-temperature (294 K) and a pressure of 17 kPa. The spectrum is fitted using the above algorithm, resulting in a temperature of 299 K and a pressure of 16.1 kPa.

Number densities of CO in the $X^1\Sigma^+(v = 0)$ state can be calculated by integrating the excitation spectrum over the $B^1\Sigma^+(v' = 0) \leftarrow X^1\Sigma^+(v'' = 0)$ two-photon excitation frequency. Due to the normalization of $\Phi(\Omega_c)$, the CO $X^1\Sigma^+(v = 0)$ number density $N_{\mathrm{CO},0}$ can be expressed as

$$N_{\mathrm{CO},0} = \frac{Q + \tau_{\mathrm{nat}}^{-1}}{Q_{\mathrm{ref}} + \tau_{\mathrm{nat}}^{-1}} \frac{P_{\mathrm{ref}}^2}{P^2} \frac{\Gamma}{\Gamma_{\mathrm{ref}}} N_{\mathrm{ref}}, \quad (6)$$

where N_{ref} is the known number density from the reference measurement. Q and Q_{ref} are the quenching frequencies at plasma and reference conditions, respectively. P and P_{ref} represent the measured laser power during the plasma and reference measurements, while Γ and Γ_{ref} are the fitted intensities for the plasma and reference measurements. The number density of CO in the $X^1\Sigma^+(v = 0)$ state can be generalised to the total CO number density N_{CO} if the vibrational temperature and type of vibrational distribution are known.

It has been reported previously that CO vibrational temperatures can exceed rotational temperatures substantially in a glow discharge [20], resulting in a significant population of higher vibrational levels. Vibrational temperatures reach up to 1400 K at 0.7 ms after the start of the pulse, resulting in up to 11% of the CO molecules to be excited above the vibrational ground-state [20]. In contrast, just before starting the plasma only 0.05% of the CO molecules is excited to higher vibrational levels at an equilibrium temperature of $T = 400$ K [20]. Total CO number densities are thus determined from the $X^1\Sigma^+(v = 0)$ number densities and the calculated population of excited vibrational levels by using the vibrational temperatures as measured by Klarenaar *et al* and assuming a Treanor vibrational distribution [20].
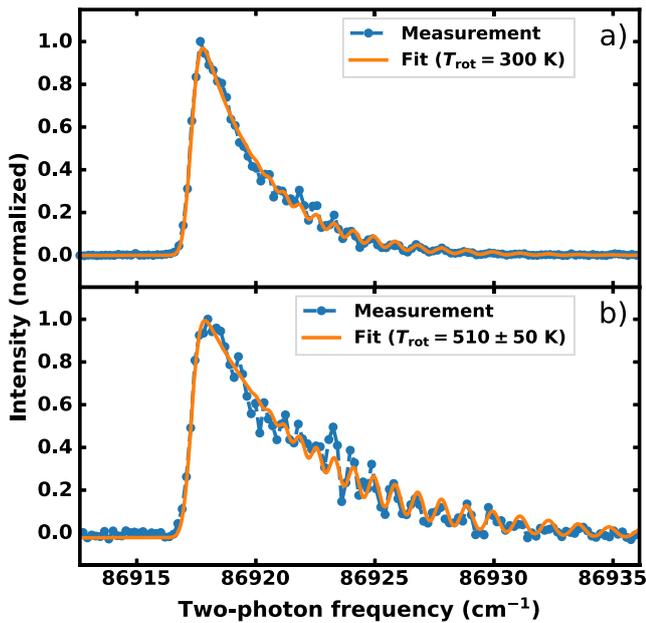
Figure 3. Measured excitation spectra and their corresponding least-squares fits at room temperature in (a) and during the cooldown period of the plasma ($t = 7.5$ ms) in (b).

5. Results

Two-photon excitation spectra were taken at different times during the plasma cycle by scanning the laser stepwise across 23 cm^{-1}, starting at an excitation frequency of 86 914 cm^{-1}, including rotational levels $0 \geqslant J \geqslant 28$. Two normalized excitation spectra measured at room temperature and during the cooldown phase of the plasma ($t = 7.5$ ms) are shown in figures 3(a) and (b), respectively. The corresponding least-squares fit for the measurement at $t = 7.5$ ms results in a rotational temperature of $T_{rot} = 510 \pm 50$ K.

Figure 3 shows a clear difference in the population over the rotational states between the excitation spectrum measured at room temperature and during the plasma cycle. By fitting the full excitation spectrum, reliable rotational temperatures can be extracted from the overall shape of the spectrum despite the noise. Furthermore, due to the increased spacing between rotational levels, (partly) resolved lines are visible at excitation frequencies above about 86 920 cm^{-1}, corresponding to $J > 10$.

Recorded rotational temperatures during the full plasma cycle are shown in figure 4(a). The start of the plasma-on phase is defined as the time origin and corresponds to a rotational temperature of $T_{rot} = 370 \pm 40$ K. Measured rotational temperatures rise quickly after starting the plasma, with the rate of heating going down until the rotational temperature reaches the maximum of $T_{rot} = 700 \pm 70$ K at $t = 4.9$ ms. When the plasma is turned off, rotational temperatures exponentially drop until reaching the minimum temperature again just before another plasma-on phase starts.

The measured rotational temperature trends are in good agreement with earlier data acquired by Klarenaar *et al* [20], while absolute rotational temperatures are slightly lower. To
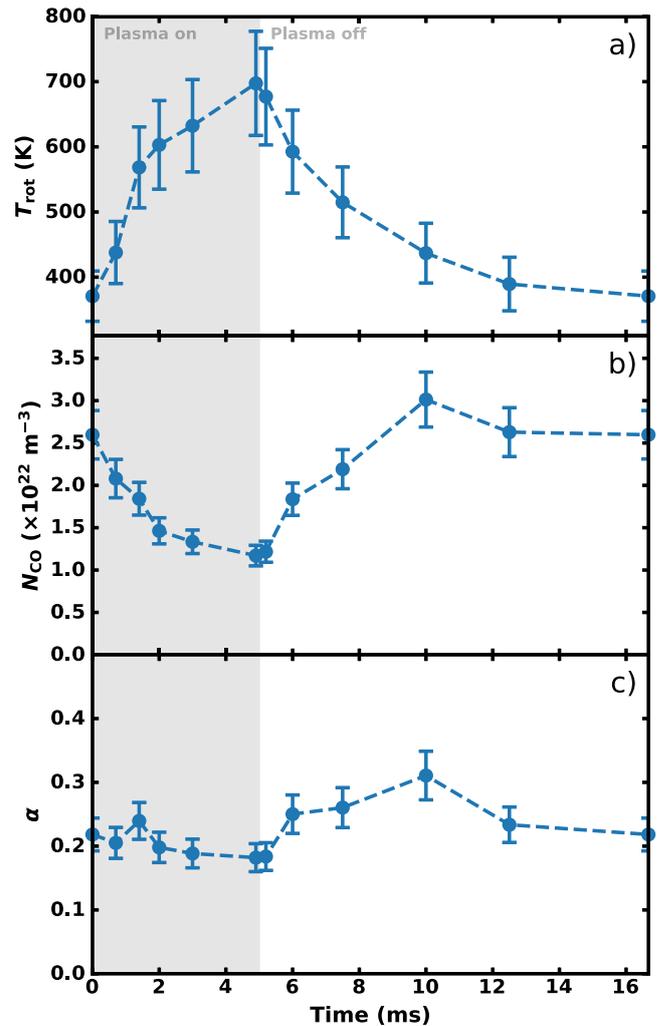

Figure 4. Measured rotational temperatures in (a), CO $X^1\Sigma^+$ number densities in (b) and corresponding plasma conversion α in (c) at different times during the plasma cycle and in the cooldown period. A 1σ fitting error is taken into account for the rotational temperature uncertainty. Additionally, an estimated 10% uncertainty is included to account for drift in laser power during an excitation scan and a difference in state-to-state Einstein A-coefficients from the $X^1\Sigma^+(v = 0)$ state average. Number density error bars only include statistical errors, while the systematic error is about 20%.

match the discharge frequency to our laser repetition rate however, the plasma-off time was increased from 10 to 11.67 ms, while the plasma-on time remained the same. As a result, our duty cycle was about 10% lower, resulting in lower overall rotational temperatures.

Figure 4(b) shows measured CO number densities, with corresponding plasma conversion shown in figure 4(c) at different times during the plasma cycle. The CO number density is not affected significantly by the initial estimation for the plasma conversion, needed for the calculation of the Stern–Volmer factor (as shown in figure 2(b)). Hence the initial estimation for the plasma conversion is taken as $\tilde{\alpha} = 0.18 \pm 0.18$, in agreement with the discussion in section 3.2. Error bars include only the statistical errors to allow easy comparison of trends during the plasma cycle. It should be noted that an additional systematic error of 20% is

present. Changes in number densities qualitatively follow the inverse trend of the measured temperatures, suggesting an isobaric expansion of the plasma volume from heating during the plasma-on phase.

Measured CO number densities, as well as the plasma conversion show similar trends to the FTIR study done by Klarenaar *et al* in a very similar plasma reactor [13, 20]. Here CO number densities were measured of about 1.9×10^{22} m^{-3} just before the plasma-on phase starts, while number densities decreased to about 1.2×10^{22} m^{-3} at the end of this plasma-on phase. Our number densities as well as the time-averaged plasma conversion of $22\% \pm 4\%$ are in fair agreement, especially when taking into account the 20% systematic error.

6. Conclusions

We have demonstrated a method to determine time-resolved rotational temperatures and absolute CO number densities in a CO$_2$ glow discharge using TALIF with a nanosecond pulsed laser. This was done by analyzing two-photon excitation spectra of CO using an appropriate fitting routine, where the full Q-branch excitation spectrum of the $B^1\Sigma^+(v'=0) \leftarrow X^1\Sigma^+(v''=0)$ transition was used. The fitting routine was checked against a previously published high signal-to-noise ratio excitation spectrum at room temperature, where good agreement was found with our fitting routine.

It has been shown experimentally that measured rotational temperatures show fair agreement with previously measured rotational temperatures. CO number densities and plasma conversion were also determined from the excitation spectrum measurements by compensating for quenching based on a rough estimation of plasma conversion and excitation of higher vibrational levels. Our number densities show good agreement with CO number densities measured in previous studies, thus showing applicability of TALIF on CO in a plasma environment.

The presented method for rotational temperature measurements is applicable to any nanosecond pulsed laser system with sufficiently narrow linewidth and even allows measuring arbitrary rotational distributions with only minor changes. Absolute CO number density measurements can be extended to any system where the local pressure and an estimate of the gas composition can be guessed. Our method will produce reliable results for CO number densities if changes in quenching frequency are limited.

Acknowledgments

Appendix. Two-photon Hönl–London factors

The two-photon selection rules restrict the allowed transitions to $\Delta J = 0, -2, +2$, corresponding to the Q, O and S branches, respectively. For two-photon absorption by CO of linearly polarized light, the corresponding Hönl–London factors are calculated by Bray *et al* [29]

$$S_{ll}^O = C\,(2J+1)\frac{1}{45}\mu_s^2\,b_{J-2,J}, \qquad (A.1)$$

$$S_{ll}^Q = C\,(2J+1)\left(\frac{1}{9}\mu_I^2 + \frac{1}{45}\mu_s^2\,b_{J,J}\right), \qquad (A.2)$$

$$S_{ll}^S = C\,(2J+1)\frac{1}{45}\mu_s^2\,b_{J+2,J}. \qquad (A.3)$$

Here μ_I^2 and μ_S^2 are invariants of the two-photon polarizability tensor, C is a constant, to allow for normalization ($S_{ll}^O + S_{ll}^Q + S_{ll}^S = 2J+1$) and $b_{J-2,J}$, $b_{J,J}$ and $b_{J+2,J}$ are Placzek–Teller coefficients given by Long *et al* [35]:

$$b_{J-2,J} = \frac{3J(J-1)}{2(2J+1)(2J-1)}, \qquad (A.4)$$

$$b_{J,J} = \frac{J(J+1)}{(2J-1)(2J+3)}, \qquad (A.5)$$

$$b_{J+2,J} = \frac{3(J+1)(J+2)}{2(2J+1)(2J+3)}. \qquad (A.6)$$

Using the fact that the sum of these Placzek–Teller coefficients equals unity, the normalization factor C can easily be determined as

$$C = \left(\frac{1}{9}\mu_I^2 + \frac{1}{45}\mu_s^2\right)^{-1}. \qquad (A.7)$$

Determining the relative values of the invariants of the polarizability tensor μ_I^2 and μ_s^2 is often done through the relative intensity of the Q-branch upon excitation by two-photon linearly and circularly polarized light, respectively. According to Bray *et al* [29], the Hönl–London factor of the Q-branch for two-photon absorption of circularly polarized light S_{cc}^Q is given by

$$S_{cc}^Q = C\,(2J+1)\,\frac{1}{30}\mu_s^2\,b_{J,J}. \qquad (A.8)$$

By combining equations (A.2) and (A.8), we find that the ratio between the Hönl–London factors for linearly and circularly polarized light is given by

$$\frac{S_{ll}^Q}{S_{cc}^Q} = \frac{2}{3}\left(1 + \frac{5}{b_{J,J}}\frac{\mu_I^2}{\mu_s^2}\right). \qquad (A.9)$$
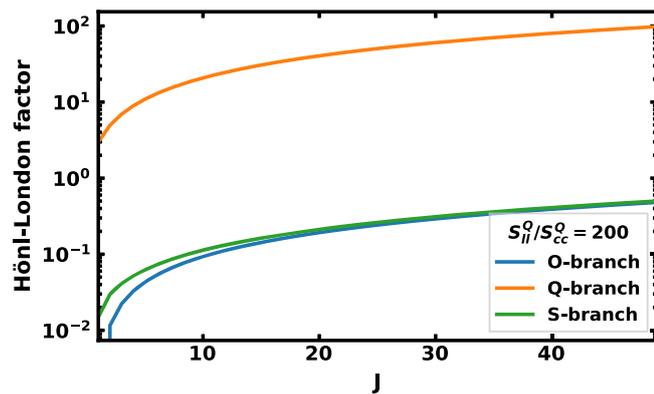
Figure A1. Calculated normalized Hönl–London factors for the O, Q and S branch, based on a Hönl–London factor ratio of linearly and circularly polarized light S_{ll}^{Q}/S_{cc}^{Q} of 200 [30], as a function of the rotational level J. This plot excludes $J = 0$, since the calculation of the ratio of the invariants of the polarizability tensor is not defined at $J = 0$. For this ratio, the Q-branch Hönl–London factor is approximately 2 orders of magnitude larger than that of the O and S branches.

It is experimentally found by Tjossem *et al* that the ratio S_{ll}^{Q}/S_{cc}^{Q} is typically over 200 [30]. Using this experimental result, the ratio between the invariants of the polarizability tensor μ_I^2 and μ_s^2 can be determined and subsequently, the Hönl–London factors for two-photon absorption of linearly polarized light can be calculated for each $J \neq 0$. The dependence of the Hönl–London factors in equations (A.1), (A.2) and (A.3) is shown in figure A1. It shows that the Hönl–London factor of the Q-branch is approximately 2 orders of magnitude larger than the line strengths of the O and S branches for any value of the rotational quantum number $J \neq 0$, which is also confirmed experimentally by the absence of the O and S branches [7, 30, 36].

ORCID iDs

M A Damen ⬤ https://orcid.org/0000-0001-6844-8838
A W van de Steeg ⬤ https://orcid.org/0000-0002-2976-7905
L M Martini ⬤ https://orcid.org/0000-0002-4501-3492
R Engeln ⬤ https://orcid.org/0000-0002-4687-7436

References

[1] Magee R M, Galante M E, McCarren D, Scime E E, Boivin R L, Brooks N H, Groebner R J, Hill D N and Porter G D 2012 *Rev. Sci. Instrum.* **83** 10D701
[2] Niemi K, Schulz-von der Gathen V and Döbele H F 2001 *J. Phys. D: Appl. Phys.* **34** 2330–5
[3] Wagenaars E, Gans T, O'Connell D and Niemi K 2012 *Plasma Sources Sci. Technol.* **21** 042002
[4] Mazouffre S, Foissac C, Supiot P, Vankan P, Engeln R, Schram D C and Sadeghi N 2001 *Plasma Sources Sci. Technol.* **10** 168–75
[5] Marinov D, Drag C, Blondel C, Guaitella O, Golda J, Klarenaar B, Engeln R, Schulz-Von Der Gathen V and Booth J P 2016 *Plasma Sources Sci. Technol.* **25** 06LT03
[6] Marchal F, Yousfi M, Merbahi N, Wattieaux G and Piquemal A 2016 *Plasma Sci. Technol.* **18** 259
[7] Linow S, Dreizler A, Janicka J and Hassel E P 2000 *Appl. Phys.* B **71** 689–96
[8] Krupenie P 1966 *The Band Spectrum of Carbon Monoxide* (Washington DC: U.S. Department of Commerce, National Bureau of Standards)
[9] Carrivain O, Orain M, Dorval N, Morin C, Legros G and Houy L M 2000 *Appl. Phys.* B **71** 689–96
[10] Rosell J, Sjöholm J, Richter M and Aldén M 2013 *Appl. Spectrosc.* **67** 314–20
[11] Maté B, Tejeda G and Montero S 1998 *J. Chem. Phys.* **108** 2676–85
[12] van den Bekerom D C M, Palomares Linares J M, van Veldhuizen E M, Nijdam S, van de Sanden M C M and van Rooij G J 2018 *Appl Opt.* **57** 5694–702
[13] Klarenaar B, Grofulović M, Morillo-Candas A, van den Bekerom D, Damen M, van de Sanden M, Guaitella O and Engeln R 2018 *Plasma Sources Sci. Technol.* **27** 045009
[14] Di Teodoro F, Rehm J E, Farrow R L and Paul P H 2000 *J. Chem. Phys.* **113** 3046–54
[15] Di Rosa M D and Farrow R L 1999 *J. Opt. Soc. Am.* B **16** 1988–94
[16] Blunt V, Lin H, Sorkhabi O and Jackson W 1995 *J. Mol. Spectrosc.* **174** 274–6
[17] Dang C, Reid J and Garside B K 1982 *Appl. Phys.* B **27** 145–51
[18] Siemsen K J, Reid J and Dang C 1980 *IEEE J. Quantum Electron.* **16** 668–76
[19] Andreev S N, Zakharov V V, Ochkin V N and Savinov S Y 2004 *Spectrochim. Acta* A **60** 3361–9
[20] Klarenaar B L M, Engeln R, van den Bekerom D C M, van de Sanden M C M, Morillo-Candas A S and Guaitella O 2017 *Plasma Sources Sci. Technol.* **26** 115008
[21] Rivallan M, Aiello Ś and Thibault-Starzyk F 2010 *Rev. Sci. Instrum.* **81** 103111
[22] van Rooij G J, van den Bekerom D C M, den Harder N, Minea T, Berden G, Bongers W A, Engeln R, Graswinckel M F, Zoethout E and van de Sanden M C M 2015 *Faraday Discuss.* **183** 233–48
[23] Brehmer F, Welzel S, van de Sanden M C M and Engeln R 2014 *J. Appl. Phys.* **116** 123303
[24] Bogaerts A, Kozák T, van Laer K and Snoeckx R 2015 *Faraday Discuss.* **183** 217–32
[25] Hempel F, Röpcke J, Miethke F and Wagner H E 2002 *Plasma Sources Sci. Technol.* **11** 266–72
[26] Di Rosa M D and Farrow R L 1999 *J. Opt. Soc. Am.* B **16** 861–70
[27] Seitzman J M, Haumann J and Hanson R K 1987 *Appl. Opt.* **26** 2892–9
[28] Dilecce G, Martini L M, Tosi P, Scotoni M and De Benedictis S 2015 *Plasma Sources Sci. Technol.* **24** 034007
[29] Bray R G and Hochstrasser R M 1976 *Mol. Phys.* **31** 1199–211
[30] Tjossem P J H and Smyth K C 1989 *J. Chem. Phys.* **91** 2041
[31] Morillo-Candas A S, Klarenaar B, Engeln R, Chatterjee A, Booth J P, Guerra V and Silva T and Guaitella O 2017 O atom kinetics in CO_2 pulsed glow discharges *33th Int. Conf. on Phenomena in Ionized Gases* p 79
[32] Gousset G, Panafieu P, Touzeau M and Vialle M 1987 *Plasma Chem. Plasma Process.* **7** 409–27
[33] Settersten T B, Dreizler A and Farrow R L 2002 *J. Chem. Phys.* **117** 3173–9
[34] Di Rosa M D and Farrow R L 2001 *J. Quant. Spectrosc. Radiat. Transfer* **68** 363–75
[35] Long D A 1977 *Raman Spectroscopy* (New York: McGraw-Hill International Book Company)
[36] Loge G W, Tiee J J and Wampler F B 1983 *J. Chem. Phys.* **79** 196–202